NUMERICAL INVESTIGATION OF DISSIPATIVE REVERSE FLOW PUMP OPERATION USING DIFFERENT SIMULATION APPROACHES

JAKUB STARECEK[1], JAKUB LIPKA[1], PROKOP MORAVEC[2]

[1]CENTRE OF HYDRAULIC RESEARCH,

[2]SIGMA Research & Development Institute,

Jana Sigmunda 313, 78349 Lutin, Czech Republic

DOI: 10.17973/MMSJ.2026_06_2025151

j.starecek@sigma.cz

Computational Fluid Dynamics (CFD) simulations are a valuable tool for hydrodynamic pump flow analyses. Recently, emphasis has been placed on the analyses of all pump modes such as turbine mode, pump mode, dissipative modes etc. Some regimes are very difficult to simulate numerically, especially transition states. These regimes must be analysed using multiple modelling approaches, considering different levels of model complexity. The CFD simulations are very useful for predicting emergency scenarios such as a pump failure, counter-pressure from the pipeline system, reverse flow, water-hammer events, etc. The future validation of simulations by experimental research is self-evident. The pump test bench is currently being prepared, for this purpose, as shown in this article. The pump test bench consists of two identical centrifugal pumps: a measured pump and feed or auxiliary (it depends on the regime in the four-quadrant characteristic) pump. These pumps, together with the pipeline system including a bypass, make it possible to measure the complete (four-quadrant) pump performance characteristics. This paper is focused on numerical simulations of the dissipative operations and non-standard pump regimes with emphasis on the analysis of the transition state between the first and second quadrant and between the second and third quadrant. The article describes and presents a comparison of different modelling approaches from the view of varying model geometry complexity. The simulation results are compared based on the performance characteristics, which could represent future test bench limits. The flow behaviour in the pump and piping system is also visualized, and it is a valuable result that can be considered in the future experiment.

KEYWORDS

Four-quadrant, Pump, Characteristics, Dissipative, Operation, CFD

1 INTRODUCTION

The hydrodynamic pumps can be classified as rotary machines operating with a positive rotor speed and a positive flow rate. The main parameters of the pumps are H [m] is the pump total head; Q represents the volumetric flow rate [$m^3 \cdot s^{-1}$] and n is the impeller rotational speed [min^{-1}] usually marked as [rpm]. Those main parameters indicate the type of the centrifugal pump (radial, diagonal or axial pump). The type of pump can be best estimated by a specific speed value. The specific speed can be calculated by the following equation (1) [Paciga 1984]:

$$n_s = 3.65 \cdot n \cdot \frac{Q^{0.5}}{H^{0.75}} \quad (1)$$

For example, the tested pump design point was set to: H = 13.8 m; Q = 11 $l \cdot s^{-1}$ and n = 1450 rpm. The specific speed of the pump is equal to n_s = 77.5 min^{-1}. This specific speed corresponds to the category of radial pumps. A cross-section of the radial pump with the definition of positive speed and positive flow is visualized in Figure 1.

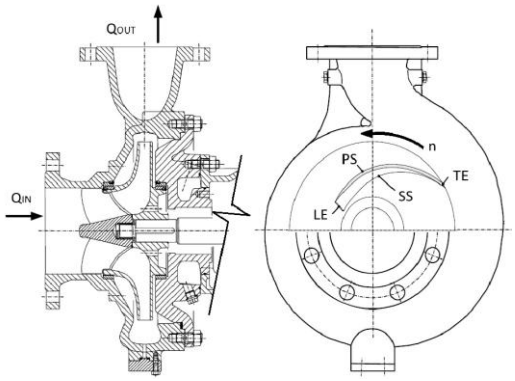

Figure 1. Cross-section of radial pump. Q_{IN} - pump inlet; Q_{OUT} - pump outlet; n - direction of rotational speed; LE - blade leading edge; TE - blade trailing edge; PS - pressure side of the blade; SS - suction side of the blade [Gulich 2014]

If the direction of the rotation and flow are reversed, the hydrodynamic pump can operate in the turbine mode. In terms of numerical modelling, turbine and pump operations are usually well understood and easily simulated, as shown for example in [Moravec 2022] or [Starecek 2022]. A pump and turbine operating principle is commonly utilized in practice, for example in a pumped-storage power plants, where pump-turbines are installed. In addition to these two main operating modes of the hydrodynamic machine, there are other regimes typically associated with transient states between the pump and turbine operation, or with emergency conditions of the pump system. There is a growing demand for determining complete pump characteristics, either through computational or experimental approaches. Particularly in the field of numerical modelling of complete characteristics, several open questions remain unanswered regarding how simulations should be performed, how the results should be evaluated and how they can be reliably validated against experimental data. The main motivation of this study is to examine several modelling approaches and to assess the differences that may arise in the results. Furthermore, the objective is to identify problematic regions of the characteristics, to develop a comprehensive understanding of the behaviour and to establish a suitable modelling methodology.

2 FOUR-QUADRANT CHARACTERISTIC

The four-quadrant characteristic can be subdivided into eight specific operating regimes, denoted as a) to h), with four of them classified as dissipative modes. Illustrative four-quadrant characteristic is shown in the Figure 2.

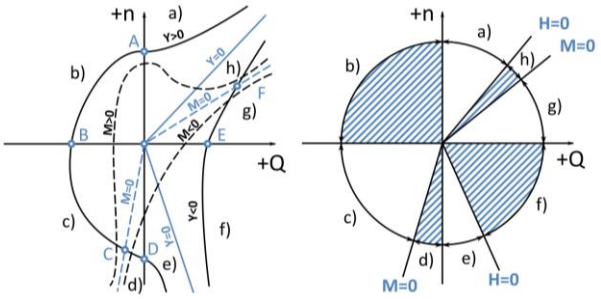

Figure 2. Four-quadrant characteristics of the hydrodynamic device [Blaha 1997]

a) **Normal pump operation** – The operating region of a hydrodynamic pump extending from a shut-off point to the full pump performance curve.
b) **Dissipative/Hydraulic brake mode** – The auxiliary pump overcomes the tested pump, resulting in a reversed flow direction.
c) **Normal turbine operation** – The operating region of a hydrodynamic machine in the turbine mode, extending from the turbine shut-off point to the runaway point.
d) **Dissipative/Hydraulic brake mode** – The auxiliary pump overdrives the tested pump at a sub-synchronous speed. This regime may not always lie strictly in the fourth quadrant; its shape depends on the specific speed of the pump.
e) **Pump operation with reverse rotation** – The tested pump operates with a reversed shaft rotation.
f) **Dissipative/Hydraulic brake mode** – The tested and auxiliary pumps overcome each other, generating a mutual hydraulic resistance.
g) **Turbine operation with reverse rotation** – The auxiliary pump drives the tested pump; the internal losses are not compensated. Series operation.
h) **Dissipative/Hydraulic brake mode** – Internal losses are compensated, and the system operates in a series configuration. [Blaha 1997]

The sign convention in all modes is summarized in Table 1.

Zone	Flow	Speed	Head	Torque
[-]	[l·s^{-1}]	[rpm]	[m]	[N·m]
a)	+	+	+	+
b)	-	+	+	+
c)	-	-	+	+
d)	-	-	+	-
e)	+	-	+	-
f)	+	-	-	-
g)	+	+	-	-
h)	+	+	-	+

Table 1. Sign convention of four-quadrant characteristics

The energetically active regions correspond to regimes a), c), e) and g), while the remaining areas b), d), f) and h) represent dissipative or braking modes. The size and shape of each region depend on the pump type, mostly on the specific speed of the pump. The transitional zone between e) and f) regimes is strongly influenced by the specific speed, and this transition region could shift between the third and fourth quadrant. From the perspective of energy transformation efficiency, the main regime a) is preferred for the pump operation, and c) is preferred for the turbine operation. The remaining regimes are generally not recommended for practical operation and are typically associated with emergency conditions, such as a failure of the feed pump. [Blaha 1997]

2.1 Construction of four-quadrant characteristics

To obtain the four-quadrant characteristic of a hydrodynamic machine, two main approaches are currently used:

a) **Experimental measurement on a hydraulic test bench** – This approach requires a highly specialized test facility. For large pumps or large turbines, a measurement across most operating regimes is practically infeasible, the same holds for devices installed on site.
b) **Numerical flow modelling** – This approach requires verification and validation of a computational accuracy, with challenges related to capturing flow behaviour and physical phenomena in transitional operating regimes.

In both cases, determining the fourth-quadrant characteristic requires analysing several operating points. It is necessary to either measure or calculate the fundamental performance parameters of the pump, such as:

a) **Total Head** H_{pump} [m] – Derived from a pressure difference between the inlet and outlet of the computational domain or test bench. As shown in equation (2).
b) **Impeller rotational speed** n [rpm] – The rotational speed is defined as a boundary condition in simulations or measured directly from a motor or frequency converter.
c) **Torque** M_k [N·m] – It is obtained directly from the numerical simulation or measured using instrumentation on the hydraulic test bench.
d) **Volumetric flow rate** Q [l·s^{-1}] or [m^3·s^{-1}] – It is defined by boundary condition or measured by a flowmeter located in the test bench.

In practice, performance curves are constructed based on the above-mentioned parameters, typically representing the relationship between the pump head, power, efficiency and flow rate or rotational speed. The first parameter is the pump head H [m], defined by the pressure difference:

$$H = \frac{\Delta p_{pump}}{g \cdot \rho} = \frac{p_{tot,OUTLET} - p_{tot,INLET}}{g \cdot \rho} \quad (2)$$

where Δp_{pump} [Pa] represents the total pressure difference between the inlet and outlet face in the computational domain or the inlet and outlet region in the measured pump. The constant ρ [kg·m^{-3}] represents the water density and g [m·s^{-2}] denotes the gravitational acceleration. The second parameter is the hydraulic efficiency:

$$\eta_h = \frac{P_o}{P} = \frac{(p_{tot,OUTLET} - p_{tot,INLET}) \cdot Q}{2 \cdot \pi \cdot n \cdot M_k} \cdot 100 \quad (3)$$

where P_o [W] represents the hydraulic output and P [W] represents the hydraulic input (hydraulic input can be written as $P = M_k \cdot \omega$, where ω represents angular velocity). Variable n [s^{-1}] is the rotational speed and Q [m^3·s^{-1}] represents the volume flow. The inverse value is used for the turbines. The IEC 60193 standard [IEC 60193] was used for the hydraulic parameter definition. Due to the complexity of experimental measurements on large pumps, there is an increasing trend toward determining four-quadrant pump characteristics through numerical simulations. To validate the numerical model, the educational test bench was developed in our laboratory. This setup allows verification of numerical simulations as well as experimental measurements under specific operating regimes of pumps. [Gulich 2014] and [Karassik 2012]

3 PUMP TEST BENCH

3.1 Measurement of complete pump characteristics

The closed hydraulic circuit is required to measure the complete performance characteristics of a pump. The circuit must be equipped with appropriate technological components, including: a tested pump, an auxiliary pump, torque and speed sensors, frequency converters, flowmeters, pressure sensors, a water reservoir and a set of fittings and valves for a construction. The following in-house design of the test

circuit was inspired by subsequent publications: Authors in [Park 2020] presented measurements of the complete pump characteristic at multiple rotational speeds and flow rates. The pump was installed in a test stand, the schematic of which was included in the article. This circuit diagram provided a basic overview of the components and layout of the test stand, and it also served as a useful reference for the design of our own setup. The paper [Bolanos 2021] focused on the measurement of the complete pump characteristic of a low-specific speed radial pump and their construction, also including a spectral analysis. The publication [Höller 2016] addresses the experimental validation of a model pump and obtaining its four-quadrant characteristic. Measured four-quadrant characteristics are compared with the results of numerical simulations. It also outlines the possibilities and limitations of a CFD analysis and physical measurement techniques. A similar area of research is also presented in following article [Xu 2022]. The article [Lu 2017] discusses the design of a test circuit for the main circulation pump. The circuit is designed for a model pump (λ = 5.6). In addition to determining the complete pump characteristics, the test setup also enables the evaluation of vapour phase effects, aiming to analyse pump parameters under emergency conditions associated with pressure drop in the circuit. The measurements were performed with gas volume fractions of 10%, 20% and 30% in the liquid.

3.2 *Pump test bench*

A hydraulic test circuit was designed using industry expertise and published research to validate the numerical simulations presented in this article. The picture of the designed circuit is shown in Figure 3.

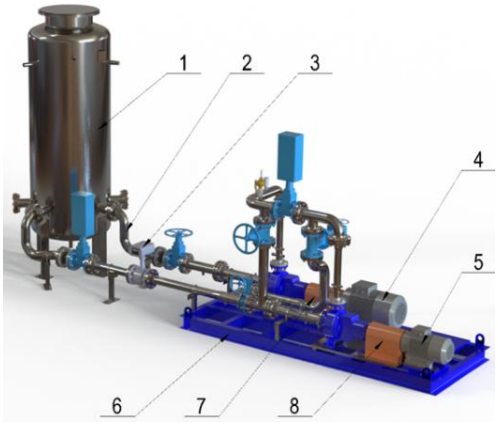

Figure 3. Visualization of pump test bench: (1) tank, (2) piping section, (3) flowmeter, (4) auxiliary pump, (5) tested pump, (6) stand base, (7) coupling and torque sensor cover. A cooler is not shown in the picture but is part of the test bench

3.3 *Tested and auxiliary pumps*

The tested pump is a centrifugal radial pump with a spiral case (volute). The feed pump is geometrically identical to the tested pump but operates at a higher rotational speed. The basic geometrical parameters of the pump and the main diameters of the monitor surfaces are visualized in the following Figure 4. The main performance parameters of the mentioned pumps in the best efficiency point (BEP) are:

Pump	Volume Flow	Head	Input	Speed
[-]	[l·s^{-1}]	[m]	[kW]	[rpm]
Tested pump	9.8	14.5	2	1450
Auxiliary pump	20	60	16.5	2950

Table 2. The main pumps parameters overview

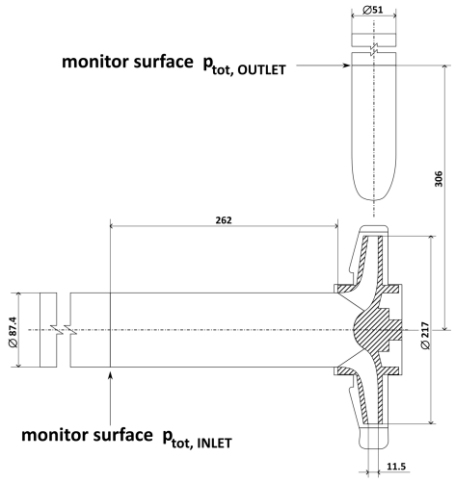

Figure 4. The main pump dimensions and geometrical parameters

4 NUMERICAL SIMULATIONS

The pump characteristics or turbine characteristics obtained by the numerical simulations are usually in a good agreement with the experiments. A few problems with simulation accuracy, convergence, etc. can occur when non-optimal regimes, dissipation regimes and other areas in the four-quadrant characteristics are simulated. Several basic findings can be deduced from the available literature, which must be considered when numerically modelling such a complex problem.

4.1 *Demands on numerical simulations*

The basic modelling approach is to use fully transient approach to capture the flow in the spaces of hydrodynamic machine. Authors in [Couziet 2011] describe the relationship between transient and stationary calculations. The simulations are also compared with measured data. The results show that in transient states, especially between the third and fourth quadrants, there is a significant distortion of the results in the stationary analysis. The distortion is mainly caused by the influence of instabilities, the increase of turbulent processes and generally poor prediction of flow conditions in the pump area. Using a transient analysis, time dependent values or phenomena can be captured, such as radial thrust, as shown in the follow-up publication [Couziet 2013]. Another key choice in terms of computational complexity and simulation accuracy is the choice of a turbulence model. In engineering practice, the SST or k-ε turbulence model is the first choice. An article [Deniz 2019] focuses on analysing the impact of these two turbulence models from the perspective of accuracy (compared with experimental data) also on pressure pulsations and their numerical damping. A potential area of our subsequent research interest is the analysis of highly turbulent and dissipative regimes using more advanced turbulence models, such as SAS, LES and others. Unfortunately, due to the computational demands, this approach can be applied only to selected operating regions rather than the entire operating range. These models significantly increase the requirements for computational meshes, and as a result, they are generally impractical in engineering applications. In general, the solution approach relies on modelling with basic turbulence models, while specific areas of interest are subjected to simulations using more accurate models. The aspects of modelling transient instabilities, typically in pump turbines is discussed in the publications [Zhang 2017] and [Gentner 2012].

4.2 3D model of pump test bench

The pump geometry was not clearly specified. 3D scanning of the impeller and volute was carried out. It was not possible to 3D scan the internal passages of the impeller due to the extremely narrow flow channels. For this purpose, a selected blade channel was filled with silicone and after its removal, it represented the shape of the blade channel. The 3D scanning process was performed in two stages: scanning of the impeller (where access with the scanning device was possible) and scanning of the silicone part of the flow channel. The same procedure was applied to the scanning of the discharge volute. The model was afterwards reconstructed, followed by an analysis of deviations. The visualization of the impeller scanning process is shown in Figure 5.

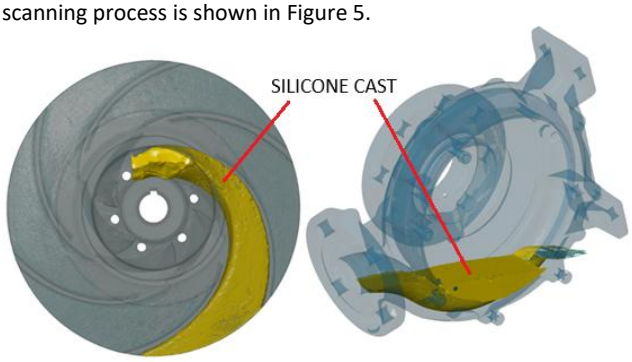

Figure 5. Impeller and spiral case with internal silicone cast

A domain which represents the side chambers and sealing rings of the pump was created for the purposes of numerical modelling and to capture volumetric losses. The pump model was extended by a calming section (stabilization section) near the inlet and outlet to improve convergence of the simulation. The axial thrust balancing holes inside the impeller body were neglected to simplify the model. The final pump geometry is shown in Figure 6.

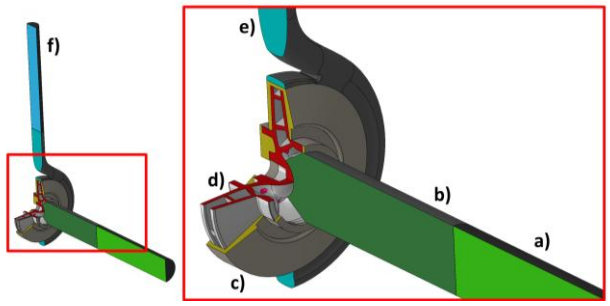

Figure 6. 3D geometry of a pump prepared for CFD analyses. a) Inlet pipe, b) suction, c) gap, d) impeller, e) spiral case, f) outlet pipe

For second and third modelling approaches, as shown in Chapter 4.3, another part of the test circuit was included in the numerical model (feed pump and whole circuit with a water tank). ANSYS TurboGrid, ICEM CFD and ANSYS Workbench Meshing were used for computational mesh generation. The mesh overview is summarized in Table 3. All parts were meshed with respect to boundary layer refinement. In a first step, an automatic wall function was chosen for boundary layer computation. A computational mesh sensitivity analysis was performed. For the "separated test pump case", three levels of mesh refinement were analysed within the range of 8 – 12 million elements. The most significant changes in mesh density were applied in the impeller and volute regions. The optimal mesh size was chosen with respect to the computational complexity. The computational meshes were tested for the pump regime (BEP).

Domain	Mesh Type	Nodes	Elements
Separated test pump case			
Impeller	Structured	1 079 352	1 002 120
Gap	Structured	3 294 900	3 151 008
Suction	Structured	1 412 749	1 382 400
Inlet Pipe	Structured	533 400	521 730
Spiral Case	Unstructured	1 101 691	2 865 764
Outlet Pipe	Structured	736 800	721 375
All Domains	-	8 158 892	9 644 397
Two pumps connected by a pipe case			
Connecting pipe	Structured	533 400	521 730
All Domains	-	16 437 784	19 405 393
Two pumps in a circuit with a tank case			
Pipes with tank	Unstructured	1 417 509	4 059 495
All Domains	-	17 855 293	23 464 888

Table 3. Mesh info overview

4.3 CFD Simulation setup

The CFD simulations were performed as fully transient simulations, where the time step was equal to 2° of impeller rotation (also for different rpm), with three to five internal iterations. The transient analyses were based on the steady-state simulations, which are also included in the results, for comparison. ANSYS CFX was used together with the Shear Stress Transport (SST) turbulence model for all simulations. Water at a temperature of T = 25°C was used as the transported medium. Mechanical losses inside the bearings and mechanical friction losses were not included in the simulations, and cavitation effects were neglected. Incompressible and isothermal fluid flow was considered. Three different approaches for numerical simulations were evaluated:

a) **Separated test pump** – The numerical analysis included only the tested pump. The mass flow rate Q_m [kg·s^{-1}] was controlled by a boundary condition. This approach was used to obtain the entire characteristic including validation with the pump manufacturer´s specification data. The total pressure was also defined as a second boundary condition. Boundary conditions depend
on the pump regime and their layout as shown in Figure 7. Both steady and transient simulations were carried out. The transient simulation was set as a benchmark against which other methods were compared.

b) **Two pumps connected by a pipe** – The connecting pipe and feed pump geometry was added to the CFD simulation. The mass flow rate was controlled by a boundary condition. The used boundary condition settings depend on pump regime as shown in Figure 8. The connecting pipe geometry was created based on the real measuring circuit. Both steady and transient simulations were carried out.

c) **Two pumps including a part of a test circuit with water tank**. The mass flow rate is generated only by the pump speed [rpm]. The tested pump speed is constant, and the feed pump speed is defined by different rpm values (as in the hydraulic laboratory by the frequency converter). Pipes and tank geometry were created based on the real measuring circuit. The mass flow rate regulation was resolved using a variable auxiliary pump speed in area b) as shown

in Figure 2. An approach using a porous domain with the constant auxiliary pump speed for the mass flow rate regulation was used in area a). A small pressure inlet (atmospheric pressure) and mass flow outlet with minimal mass flow rate were added to satisfy continuity convergence. A free-slip wall at the top of the tank was selected to mimic a free water surface behaviour. Due to high time requirements only the steady-state analysis was carried out. The visualization of the boundary conditions is shown in Figure 9.

Boundary conditions for different approaches are visualized in figures below:

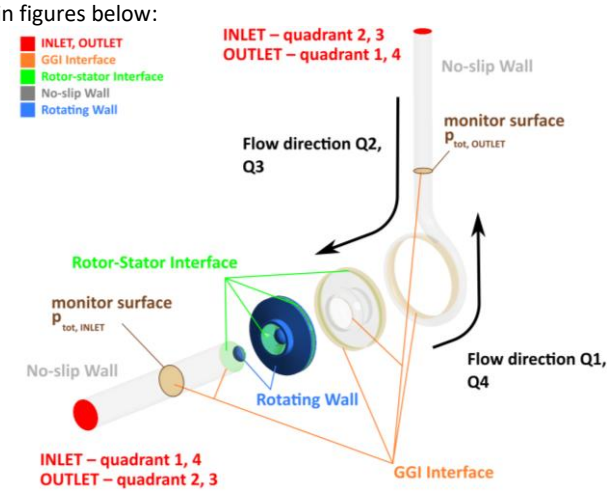

Figure 7. Boundary conditions – a) Separated test pump

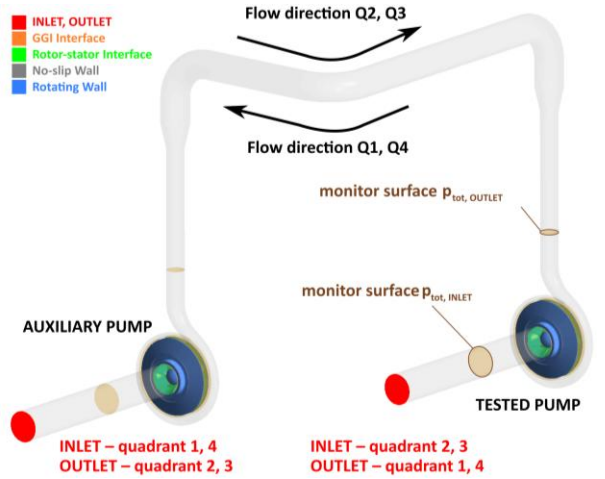

Figure 8. Boundary conditions – b) Two pumps connected by a pipe

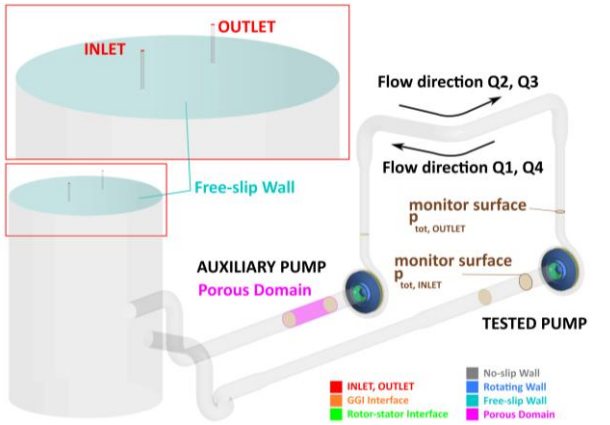

Figure 9. Boundary conditions – c) Two pumps in circuit with a tank case including porous domain

In case c), the porous domain was used as a substitute for a control gate valve to regulate the flow rate in the hydraulic test circuit. Ansys CFX [Ansys 2024] enables control of the behaviour of the porous domain using three parameters – area porosity, permeability and loss coefficient. Constant values of volume porosity (0.95) and loss coefficient (0.1 m^{-1}) were set. To achieve required flow rate permeability value was changed between $2 \cdot 10^{-10}$ to $1 \cdot 10^{-8}$ m^2.

5 RESULTS

5.1 *Tested and auxiliary pump comparison*

Experimental data obtained from the manufacturer's product catalogue and baseline CFD simulations (transient separated test pump) were compared in Figure 10 - 12.

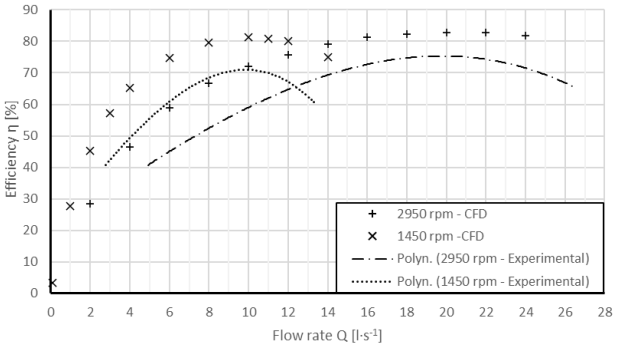

Figure 10. Q-η characteristic of both pumps

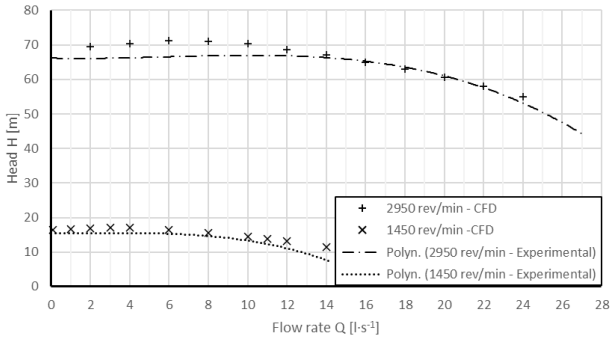

Figure 11. Q-H characteristic of both pumps

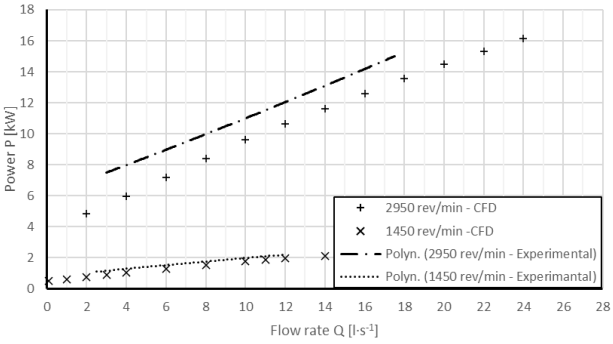

Figure 12. Q-P characteristic of both pumps

The CFD results show higher efficiency values than the experimental data. This fact can be attributed to the neglect of the mechanical friction losses in the bearings and seal, as well as the omission of the volumetric losses through the seals and the exclusion of the balance holes in the impeller. Regardless of that trend, similarities between the CFD results and experimental data can be observed for both the 1450 rpm and 2950 rpm cases. The CFD values of the pump head are also slightly higher. This may be caused by the same simplification factors as were described in a connection with the efficiency. An almost identical trend can be observed in the 1450 rpm case, whereas in the 2950 rpm case the trends seem to correspond near the BEP, but in the lower flow rates the data start to diverge. In the case of the power, similar trends between the CFD results and experiment can be observed. The CFD values

tend to be lower due to the neglection of the losses where higher power is needed to cover the real losses in the experiment. Overall, trends correspond well in the areas near the Best Efficiency Point (BEP), while a small offset in variable values can be attributed to the neglect of mechanical and volumetric losses in the CFD model.

5.2 *Four-quadrant characteristics*

The four-quadrant characteristic, based on all points obtained by the numerical simulations with the separated tested pump, was carried out in the first step. From this characteristic, it is possible to broadly evaluate the operating regions that define the performance limits of the computational test setup, especially for the auxiliary pump and, more significantly, for the tested pump. All transitional states were also detected: two states with zero total head (H = 0 m) and two states with zero torque (M_k = 0 N·m), which also defined the pump and turbine working areas. These findings are valuable for future experiments on the hydraulic test bench, as the indication of where specific transition states are likely to occur. Two main transition states were defined as our field of interest:

- Between (a) normal pump operation and (b) dissipative regime. There is a transition state with zero volumetric flow rate, with intense turbulence areas, especially in the dissipative regime, marked by red rectangle in Figure 13.
- Between (b) dissipative regime and (c) normal turbine operation. At zero rpm, the system passes through a transition state in which the dissipative regime becomes highly turbulent. On the other hand, the turbine accelerates up from zero rpm to an optimum, marked by blue rectangle in Figure 13.

Both of transition states were evaluated with the feed pump, and the results were compared.

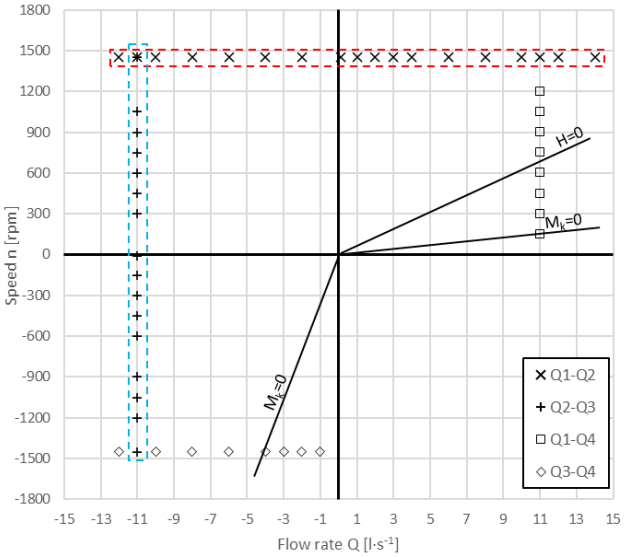

Figure 13. Q-n characteristic of all analysed points; a) separated pump approach, areas of interest highlighted by rectangles

5.3 *Different approach of modelling – (a) to (b) transition state*

In this region, a transition state occurs in which the auxiliary pump overpressures the tested pump. In practice, the pumps oscillate between pumping and dissipative modes. This is a highly transient process with a relatively long period, which has not yet been accurately captured in the CFD simulations, mainly due to limitations of the modelling approach. The third approach c), including the free water surface (using VOF) could be a promising way to simulate this transitional state with respect to the oscillating process. This is the subject of our further research. From the results, it is evident that the head curve in the pump operating mode is in this case not dependent on the type of numerical simulation. Results from transient and steady-state simulations are similar (see Figure 14 – right side). However, the input power and torque already show a noticeable scatter of values within the transition region (see Figure 15 – right side). When the transient simulations are used, the results converge, and the trends of the curves become identical. The scatter of the input power values typically increases in the region of instability of the Q-H characteristic. In the optimal pump operating regime (flow area Q = 6 - 11 l·s^{-1}), turbulent effects such as flow separation from the blades and vortex formation, or local backflow within the pump components are minimized. The tested modelling approaches show good agreement.

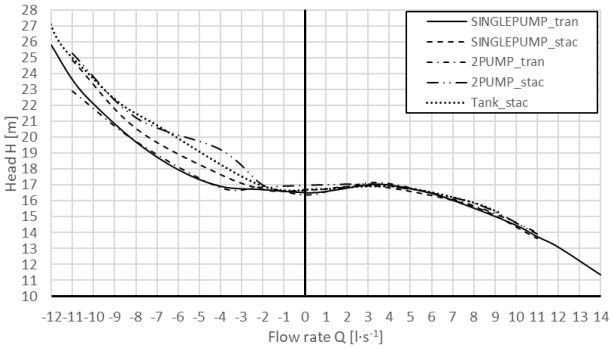

Figure 14. Q-H characteristics with different modelling approach

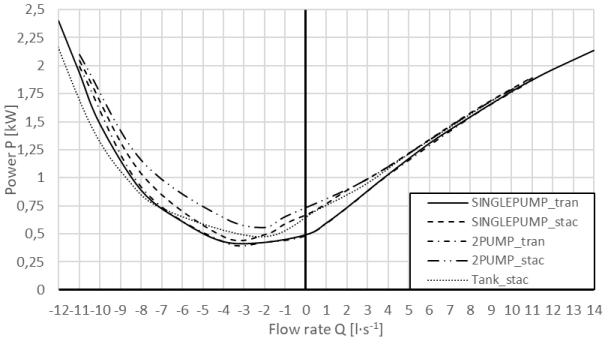

Figure 15. Q-P characteristics with different modelling approach

The situation changes significantly with the transition to the second quadrant (see Figure 14 and Figure 15 – left sides), where a considerable scatter of values appears depending on the different modelling approach. The dissipative region is characterized by a pronounced flow recirculation at the suction of the tested pump. A substantial increase in the circumferential velocity component occurs. This circumferential velocity component ultimately affects the outlet boundary condition at the pump inlet. For this reason, the entire hydraulic circuit was modelled to avoid a distortion of the boundary. Strong flow recirculation is visualized in Figure 16. Circumferential velocity magnitude v_{circ} [m·s^{-1}] can be defined as:

$$v_{circ} = \sqrt{v_x^2 + v_y^2} \qquad (4)$$

where v_x [m·s^{-1}] represents the x-component of the velocity and v_y [m·s^{-1}] represents the y-component of the velocity, from the point of view of the global axis definition. The same approach of recirculation flow visualization was used in [Moravec 2022]. In Figure 17, a flow reversal within the volute casing can be observed. The rotor speed remains constant. In the region of positive flow rates (pump operation), the flow is without significant turbulence. In the transition and dissipative regions (negative flow rates), massive vortex formation occurs in the impeller area. All the energy supplied to the pump rotor is dissipated.

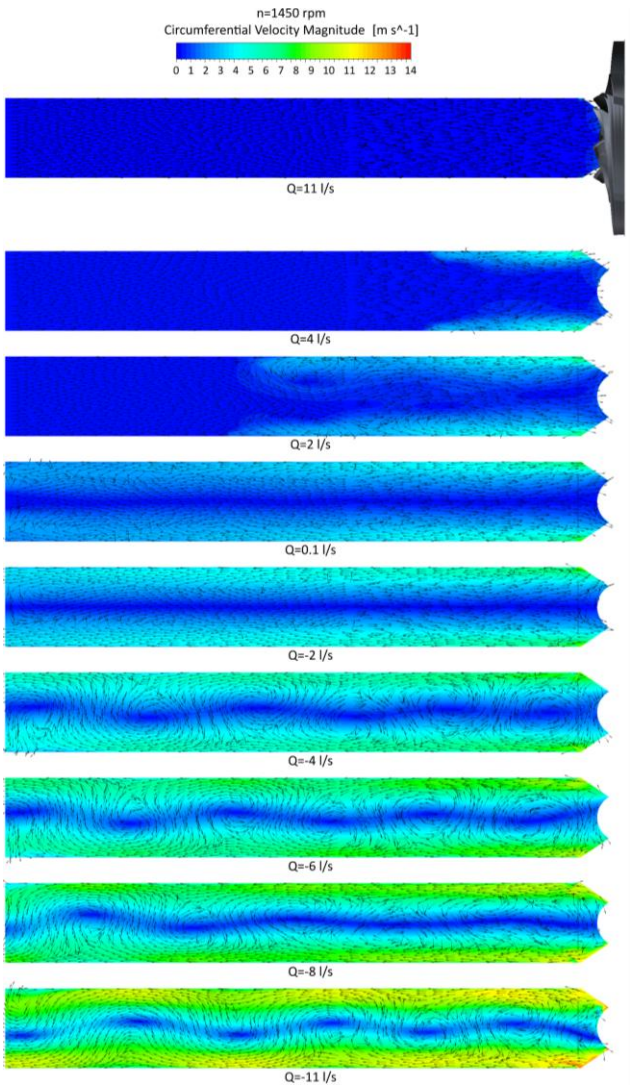

Figure 16. Circumferential velocity magnitude contours across different regimes at n = 1450 rpm in Inlet and suction pipe

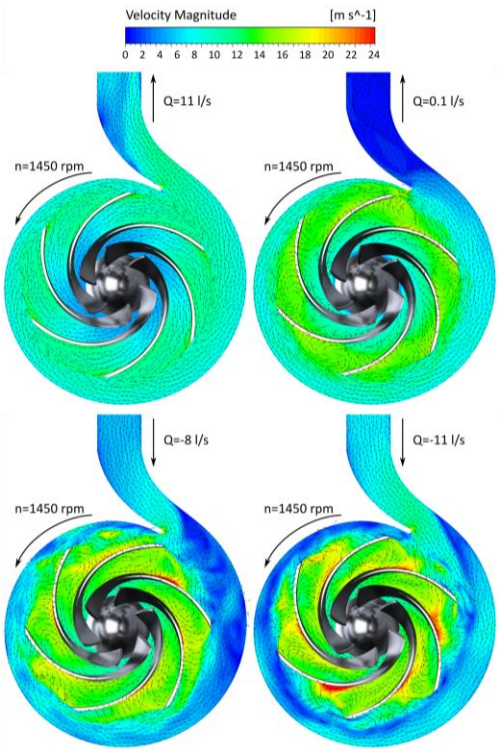

Figure 17. Velocity magnitude contours across different regimes in spiral case (n = 1450 rpm)

5.4 Different approach of modelling – (b) to (c) transition state

In this transition state, the impeller of the tested pump comes to a complete stop. For this reason, the input power in the transition region is zero, due to the zero rotational speed of the rotor; however, the torque action on the pump shaft remains non-zero, as shown in the denominator of Equation (3). In the Figure 18 and Figure 19, the main performance parameters of the pump in the dissipation regime and turbine regime are shown.

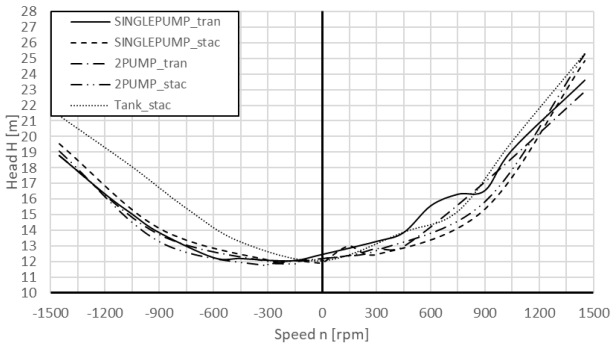

Figure 18. n-H characteristics with different modelling approach

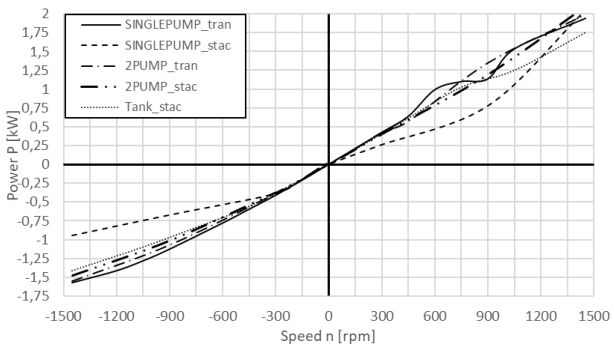

Figure 19. n-P characteristics with different modelling approach

The results indicate that the spread of the performance parameters for different modelling approaches is most pronounced in the dissipative regime within the second quadrant (positive rpm). The transition to the turbine regime, accompanied by a reduction in turbulence intensity inside the pump, leads to a decrease in the parameter dispersion in the turbine regime. Within the rotational speed range of 450 – 1050 rpm, the instability of the n – H and n – P curves can be observed (simulation involving only the test pump), the other approaches do not predict such instability. The trend of the characteristics obtained from the steady-state simulation of the entire test circuit does not correspond to the other trends and should be further verified and refined by a transient analysis. The highest level of agreement among the results is observed in the transition region between the second and third quadrants. The transition region is relatively insensitive to the complexity of the numerical model, while its sensitivity increases toward the dissipative regime where turbulence intensity is high. Flow visualization reveals a recirculation zone within the dissipative region, which gradually vanishes as the operation transitions into the turbine mode. In this regime, additional flow phenomena appear, as illustrated in Figure 20. Figure 21 shows a gradual decrease in rotational speed within the dissipative regime, followed by a transition to the turbine mode. The flow inside the volute and impeller becomes progressively stabilized, and the strongly turbulent regions in the inter-blade passages gradually disappear.

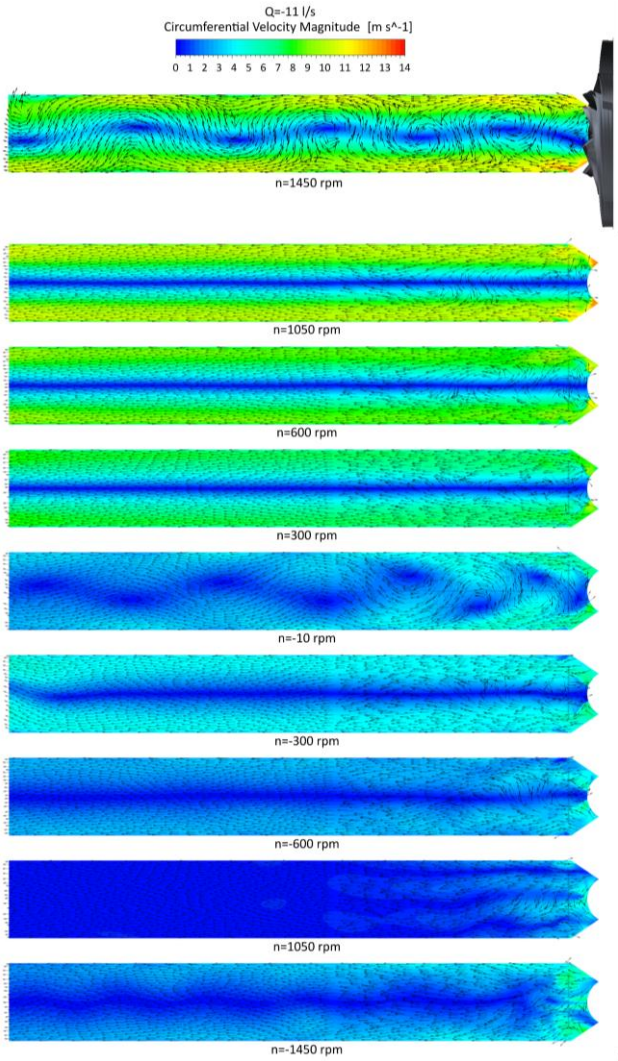

Figure 20. Circumferential velocity magnitude contours across different regimes at Q = -11 l·s^{-1} in Inlet and suction pipe

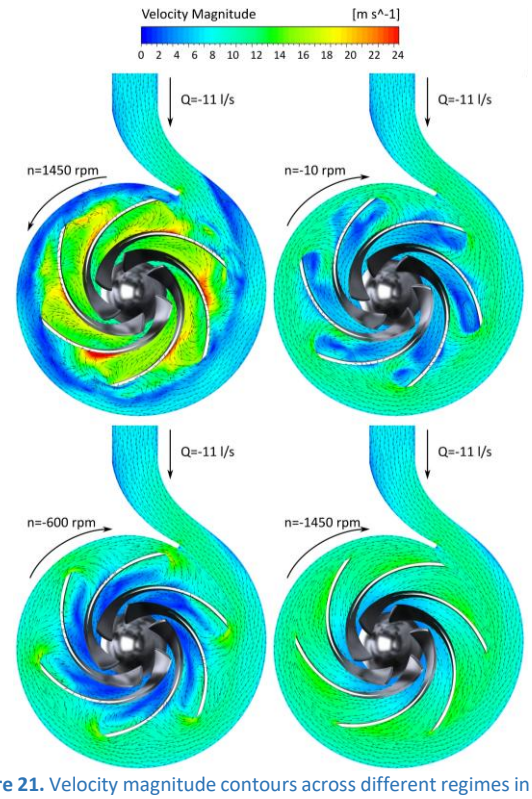

Figure 21. Velocity magnitude contours across different regimes in spiral case (Q = -11 l·s^{-1})

6 CONCLUSIONS

The following conclusions and recommendations can be formulated based on the results obtained by the numerical simulations:

- it is possible to determine the performance parameters that the tested pump will achieve. Particularly regarding the device´s power input or output and the associated mechanical stress limits of the pump system (all obtained data are not presented in this article). The data from simulations will be used as base for future measurements and future comparison.
- The performance parameters of the pump obtained by the CFD simulations are in good agreement with the catalogue data. The differences in the parameters are caused by the mechanical and volumetric losses, which were not considered in the simulations. The difference between the CFD data and catalogue data can also be caused by dimensions of the tested pump, which falls into the category of very small pumps. The performance curve trends obtained by CFD simulations exhibit a consistent trend with the catalogue data.
- The results show that regions without highly turbulent flow can be accurately simulated using simple steady-state simulation, such as pump or turbine optimal operating point. Good agreement was also observed in the transition region between the second and third quadrants, where a stationary impeller with zero input power was simulated.
- In general, all used modelling approaches yield comparable results, at least with respect to the trends of the resulting characteristics. The absolute differences in the obtained values are relatively large in some regions (especially in the second quadrant). The results can still be considered satisfactory given the complexity of the flow within the pump domain.
- The dissipative region in the second quadrant, on the other hand, must be simulated at a higher level of complexity as a time-dependent analysis, with particular attention to the selection of boundary conditions. A significant issue arises from the pronounced circumferential velocity component at the inlet of the tested pump, which can, in certain operating modes, affect the entire measurement circuit.
- For the simulation of the fourth quadrant, it is necessary to modify the configuration of the test rig (by using a bypass). This modification would fundamentally change the type of the problem in terms of geometry. This will be the subject of a further investigation. The results obtained from the CFD simulations will serve as a basis for a subsequent experimental verification, and the numerical simulations will be validated accordingly.
- The simulations will subsequently be verified through measurements performed on the hydraulic test circuit. In the future, it is planned to replace certain pipe sections with transparent segments to visually validate the flow characteristics and observe additional phase (cavitation). Also, it is necessary to include a second phase in the numerical analysis in the next step of our research.
- Further research directions in the field of numerical modelling have also emerged from this work.

The partial experience obtained from these simulations will be utilized in future studies of other operating regimes. For example, by using a bypass configuration to simulate the fourth quadrant.

The results obtained from the simulations will be utilized for comparison with experimental data to be collected in the upcoming year. The CFD analysis offers valuable information regarding the flow behaviour and the dynamics of the measurement circuit. During the simulations, several additional directions for further improvement in numerical modelling of the complete pump characteristics were identified. These include, for example, the free water surface (VOF approach) in the water reservoir within the circuit, or the extended use of porous domains to simulate flow throttling. Furthermore, the inclusion of the cavitation effect in the system represents a significant direction for future accuracy improvements of the numerical model.

ACKNOWLEDGMENTS

Computational resources were provided by the e-INFRA CZ project (ID:90254), supported by the Ministry of Education, Youth and Sports of the Czech Republic.

This research was funded by the Ministry of Industry and Trade of the Czech Republic, funding ID 28645413.

This research was supported the Czech Ministry of Education, Youth and Sports grant CZ.02.01.01/00/23_021/0008954.

REFERENCES

[Blaha 1997] Blaha, J., Brada, K. Prirucka cerpací techniky.Vyd.1. Praha: CVUT, 1997, 289 s. : il. ; 21cm. ISBN80-01-01626-9.

[Paciga 1984] Paciga, A., Strycek O., Ganco M. Cerpacia technika. Bratislava: Alfa, 1984.

[Gulich 2014] Gulich, J.F. Centrifugal pumps. Heidelberg: Springer, 2014. ISBN 978-3-642-40113-8.

[Karassik 2012] Karassik, I., Mcguire, J.T. Centrifugal pumps. Springer Science & Business Media, 2012. ISBN 978-1-4615-6606-9.

[Moravec 2022] Moravec, P., Zavadil, L., Starecek, J., Kratky, T., Danek, T., Inlet recirculation in partload regimes-radial pump. Online. MM Science Journal. 2022, vol 2022, no.2, s 5629-5637. ISSN 1803-1269. https://doi.org/10.17973/mmsj.2022_06_2022060.

[Starecek 2022] Starecek, J., Prejda, V., Moravec, P., Abrahamek, P., Zavadil, L., Kratky, T., Dolakova, H., Maslan, M., Numerical investigation of the impeller blades, manufactured by metal 3D printing technology with internal structures. Online. MM Science Journal. 2022, vol 2022, no.2, s 5689-5698. ISSN 1803-1269. https://doi.org/10.17973/mmsj.2022_06_2022082.

[IEC 60193] International Standard IEC 60193: Hydraulic pumps, and pump-turbines – Model acceptance tests. International Electrical Commission. Genf. 1999.

[Park 2020] Park, J.S., Kim, J.W., Lee, J.S. Complete and homologous pump characteristics for a reactor coolant pump. Online. Nuclear Engineering and Design. 2020, roč. 357. ISSN 00295493. https://doi.org/10.1016/j.nucengdes.2019.110425. [cit. 2023-11-28]

[Bolanos 2021] Bolanos, H.D., Botero, F. Four quadrant characterization of hydrodynamic phenomena in a low specific speed centrifugal pump. Ing. Univ. Vol. 25, 2021. https://doi.org/10.11144/Javeriana.isued25.fchp

[Höller 2016] Höller, S., Benigni, H., Jaberg, H. Investigation of the 4-quadrant behaviour of a mixed flow diffuser pump with CFD methods and test rig evaluation. Online. IOP Conference Series: Earth and Environmental Science. 2016, roč. 49, č.3. ISSN 1755-1307.https://doi.org/10.1088/17551315/49/3/032018.

[Xu 2022] Xu, L.,Liu, D., Li, Z., Zhao, X., Liu, X. Experimental and numerical simulation research on flow characteristics of model pump-turbine in four-quadrant operating quadrants. Online. Journal of Energy Storage. 2022, roč.54. ISSN 2352152X. https://doi.org/10.1016/j.est.2022.105083

[Lu 2022] Lu, Y., Zhu, R., Wang, X., Fu, Q., Li, M. et all. Study on gas-liquid two-phace all-characteristics of CAP1400 nuclear main pump. Online. Nuclear Engineering and Design. 2017, roč. 319, s. 140-148. ISSN 00295493.https://doi.org/10.1016/j.nucengdes.2017.05.001.

[Couziet 2011] Couziet, A., Gros, L., Pierrat, D., Landry, L. 4-Quadrant characteristics of centrifugal pump and unsteady computations of abnormal operating point. Luc 2011. Proceedings of the Twenty-Seventh International Pump Users Symposium September 12-15, 2011 Houston, Texas

[Couziet 2013] Couziet, A., Gros, L., Pierrat, D., Characteristics of centrifugal pumps working in direct or reverse mode: Focus on the unsteady radial thrust. Online. International Journal of Rotating Machinery. 2013. 2013, s 1-11. ISSN 1023-621X. https://doi.org/10.1155/2013/279049.

[Deniz 2019] Deniz, S., Rio, A.D., Casartelli, E., Experimental and numerical investigation of the speed-no-load instability of a low specific speed pump-turbine with focus on the influence of turbulence models. Online. IOP Conference Series: Earth and Environmental Science. 2019, roč. 240. ISSN 1755-1315. https://doi.org/10.1088/1755-1315/240/8/082005.

[Zhang 2017] Zhang, Y., Wu, Y. A review of rotating stall in reversible pump turbine. Online. Proceedings of the institution of Mechanical Engineers, Part C: Journal of Mechanical Engineering. Science. 2017, roč. 231, č. 7, s 1181-1204. ISSN 0954-4062. https://doi.org/10.1177/0954406216640579

[Gentner 2012] Gentner, Ch., Sallaberger, M., Widmer, Ch., Braun, O., Staubli, T. Numerical and experimental analysis of instability phenomena in pump turbines. Online. IOP Conference Series: Earth and Environmental Science. 2012. roč 15, č. 3 ISSN 1755-1307.https://doi.org/10.1088/1755-1315/15/3/032042

[Ansys 2024] ANSYS, Inc. ANSYS CFX User´s Guide, Release 2024, R2

CONTACTS:

Ing. Jakub Starecek, Ph.D.
Department of Hydraulic Research
CENTRE OF HYDRAULIC RESEARCH, Jana Sigmunda 313, 783 49 Lutin
j.starecek@sigma.cz